Applied Physics Letters

Coherent thermal emission near 10.6 μm mediated by localized phonon-polariton modes in microparticle arrays

Cite as: Appl. Phys. Lett. **106**, 031110 (2015); https://doi.org/10.1063/1.4906357
Submitted: 13 December 2014 . Accepted: 09 January 2015 . Published Online: 21 January 2015

Giuseppe D'Aguanno

Coherent thermal emission near 10.6 μm mediated by localized phonon-polariton modes in microparticle arrays

Giuseppe D'Aguanno[a)]
Department of Computer Science and Electrical Engineering, University of Maryland, 1000 Hilltop Circle, Baltimore, Maryland 21250, USA

(Received 13 December 2014; accepted 9 January 2015; published online 21 January 2015)

I study the thermal emission properties of periodic multilayer arrays of subwavelength particles made of silicon carbide embedded in a zinc selenide host medium. A unique interplay between the intrinsic phonon-polariton resonance of the single particle and the field thermally emitted from the different arrays of particles gives rise to a comb of highly coherent absorption/emissivity lines around 10.6 μm, ensuing ideal conditions to achieve long-wave infrared coherent sources. [http://dx.doi.org/10.1063/1.4906357]

Mid-wave and long-wave infrared (IR) coherent sources are essential for a great variety of applications ranging from information technology and industrial process control to spectroscopy and frequency metrology.[1] Molecular gases, environmental pollutants, and several explosive agents have strong absorption fingerprints in the mid-wave and long-wave IR. Military applications of mid-wave and long-wave IR lasers include their use as countermeasures against heat-seeking missiles. Beside CO_2 lasers, narrow-band sources in the mid-wave and long-wave-IR are restricted to light-emitting diodes (LEDs) and quantum cascade lasers, both being characterized by various fabrication challenges. In the last decade, many theoretical and experimental efforts have been devoted to the possibility of manipulating the black-body emission,[2] which is inherently broadband and incoherent, to realize narrowband mid-wave and long-wave IR thermal light sources. Most of the approaches rely on the excitation of surface waves such as phonon-polaritons in gratings made of polar materials like Silicon Carbide (*SiC*),[3,4] plasmon-polariton in metallic gratings,[5,6] and leaky surface waves in semiconductor photonic crystals films.[7] Other important approaches exploit instead the metamaterial properties of metallic structures[8–10] or pre-fractal configurations of one-dimensional, multilayers.[11]

In this letter, we present a study of the thermal emissive properties of periodic multilayer arrays of subwavelength particles made of *SiC* embedded in a Zinc Selenide (*ZnSe*) host medium. In particular, we concentrate on the "Reststrahlen band" of the *SiC*, which is the spectral region between the longitudinal ($\sim$10.2 μm) and the transverse ($\sim$12.6 μm) optical phonon, where the *SiC* relative permittivity is negative (like a metal below its plasma frequency), allowing therefore the excitation of localized phonon-polariton modes in the particles, essentially in the same way as localized plasmon-polariton modes are coupled with metallic nanoparticles in the visible range. In the vicinity of the intrinsic phonon-polariton resonance of the *SiC* microparticles, a comb of highly coherent absorption/emissivity lines is formed around 10.6 μm for properly designed samples. It is important to note that a bulk of *SiC* in the "Reststrahlen band" is characterized by high reflectivity, and therefore inefficient emissivity, due to its metallic behavior. Here, we devise a way to manipulate and strongly enhance *SiC* thermal emission in a frequency range where it is generally believed to be a poor emitter.

In Fig. 1, we show the structure investigated: A finite structure made of N layers of *SiC* spherical microparticles separated by a distance of d, embedded in the *ZnSe* background medium of thickness $L = (N+1)d$, and closed on the back by a metallic mirror. Each layer is formed of a rectangular array of microparticles with periodicity along the x and y directions, respectively, Λ_x and Λ_y. Using a Green function approach, as outlined in Ref. 12, and in the regime where the incident wavelength is much longer than the periodicity of the particle array (homogenization limit) $\lambda \gg (\Lambda_x, \Lambda_y)$, the electromagnetic properties of the structure can be fully calculated by a simple transfer matrix model involving only the fundamental (0-*th*) diffracted order from each layer of nanoparticle[13]

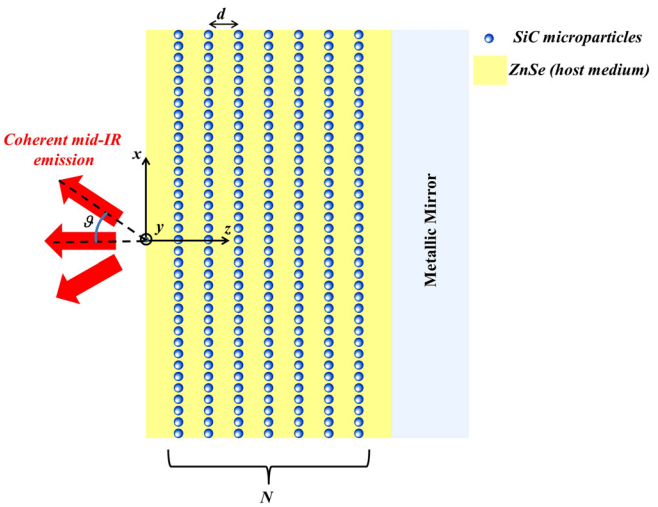

FIG. 1. Finite multilayer structure made of N layers of *SiC* microparticles separated by a distance of d and embedded in a *ZnSe* background medium. Each layer is formed of a rectangular array of microparticles with periodicity along the x and y directions, respectively, Λ_x and Λ_y. The structure is closed on the back by a metallic mirror. ϑ is the emission angle taken with respect to the normal at the input surface oriented outward.

a)E-mail: giusdag@umbc.edu

$$\begin{pmatrix} 1 \\ r \end{pmatrix} = \hat{M}_{in}\hat{S}^{N}\hat{M}_{metal}\hat{M}_{out}\begin{pmatrix} t \\ 0 \end{pmatrix}, \tag{1a}$$

where $\hat{S}$ is the transfer matrix of the elementary cell of the multilayer

$$\hat{S} = \begin{pmatrix} \dfrac{e^{-iqd}}{t_{0,0}} & -\dfrac{r_{0,0}}{t_{0,0}}e^{-iqd} \\ \dfrac{r_{0,0}}{t_{0,0}}e^{iqd} & \left(t_{0,0} - \dfrac{r_{0,0}^2}{t_{0,0}}\right)e^{iqd} \end{pmatrix}. \tag{1b}$$

$\hat{M}_{in}$ is the matrix that links the amplitudes of the fields at the first interface, $\hat{M}_{metal}$ is the transfer matrix of the metallic layer on the back of the structure, $\hat{M}_{out}$ is the matrix that links the amplitudes of the fields at the last interface, r and t are, respectively, the reflection and transmission coefficient of the structure, $q = \sqrt{k_0^2\varepsilon_{ZnSe} - k_x^2}$ is the wavevector along the z-axis (propagation direction) in the host medium, k_x is the transverse wavevector, and $r_{0,0}$ and $t_{0,0}$ are, respectively, the reflection and transmission coefficients of the fundamental diffracted order from a single layer of nanoparticles embedded in *ZnSe*.

The dispersion properties of the *SiC* can be described using the standard form of the dielectric function for polar crystals[4,14]

$$\varepsilon_{SiC}(\nu) = \varepsilon_{\infty}\left[1 + \frac{\nu_{LO}^2 - \nu_{TO}^2}{\nu_{TO}^2 - \nu^2 - i\Gamma\nu}\right], \tag{2}$$

where $\varepsilon_{\infty} = 6.7$ is the relative dielectric constant due to the electronic polarizability (at frequency well below any electronic transition resonance), $\nu_{LO} = 969\,\mathrm{cm}^{-1}$ ($\lambda_{LO} = 10.32\,\mu$m) is the frequency of the longitudinal optical phonon, $\nu_{TO} = 793\,\mathrm{cm}^{-1}$ ($\lambda_{TO} = 12.61\,\mu$m) is the frequency of the transverse optical phonon, and $\Gamma = 4.76\,\mathrm{cm}^{-1}$ is the damping. The relative electric permittivity of *ZnSe* (ε_{ZnSe}) has been modeled according to the data of Ref. 15. *ZnSe* has been chosen because of its remarkable wide transparency window, from $\sim$0.6 μm to $\sim$18 μm, and high melting point ($\sim$1800 K), characteristics that indeed make it widely used for the optics of high power CO_2 lasers at 10.6 μm. Also *SiC* can withstand extremely high temperatures with a melting point at $\sim$3000 K, ideal for thermal applications. Here, we operate in the "Reststrahlen band" of the *SiC*, which, as already mentioned, is the spectral region between the longitudinal ($\sim$10.2 μm) and the transverse ($\sim$12.6 μm) optical phonon, where the *SiC* relative permittivity is negative. In this region, localized phonon-polariton modes for the single particle can be excited according to the following expression for the single particle polarizability (including the correction term dictated by the optical theorem):[16]

$$\alpha = \left[\left(4\pi r_s^3\varepsilon_{ZnSe}\frac{\varepsilon_{SiC} - \varepsilon_{ZnSe}}{\varepsilon_{SiC} + 2\varepsilon_{ZnSe}}\right)^{-1} - i\frac{k_{ZnSe}^3}{6\pi\varepsilon_{ZnSe}}\right]^{-1}, \tag{3}$$

where r_s is the particle radius and $k_{ZnSe} = k_0\sqrt{\varepsilon_{ZnSe}}$ with $k_0 = 2\pi/\lambda$ being the vacuum wavevector. The single particle polarizability is resonantly enhanced at $\mathrm{Re}(\varepsilon_{SiC}) \cong -2\varepsilon_{ZnSe}$ (Fröhlich condition).[17] Fig. 2 summarizes the dispersive properties of the materials used.

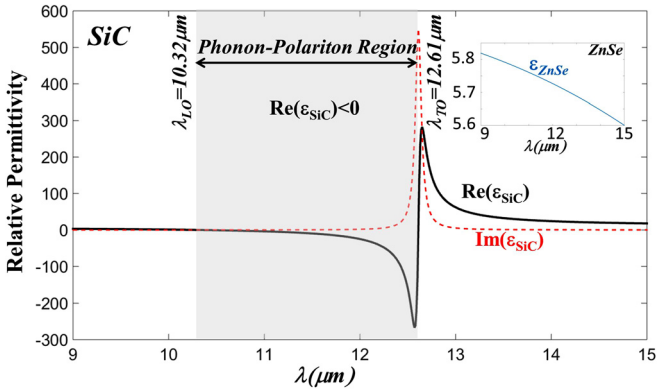

FIG. 2. Relative electric permittivity of *SiC* vs. wavelength. Inset: Relative electric permittivity of *ZnSe* vs. wavelength.

The total emissivity (ε) is defined as usual[2]

$$\varepsilon(\lambda,\vartheta) = \frac{1}{2}[\varepsilon_{TE}(\lambda,\vartheta) + \varepsilon_{TM}(\lambda,\vartheta)], \tag{4}$$

where $\varepsilon_{TE/TM} = 1 - R_{TE/TM}$ and $R_{TE/TM}$ is the reflectance (reflected power divided incident power) of the sample for *TE/TM* polarization (*s/p* polarization). Note that in our case, the structure is closed on the back by a metallic mirror so that the transmittance T is practically negligible. In the calculations, we have used an *Ag* mirror of thickness of 250 nm. The dispersion of the *Ag* is modeled with a lossy Drude model that fits the experimental data reported in Ref. 18.

In Fig. 3, we show the emissivity in the "Reststrahlen band" at $\vartheta = 0°$ as function of the wavelength (λ) and the distance (d) between the particle layers. The structure is made of $N = 25$ layers of particles with radius $r_s = 500$ nm. The particles on each layer are ordered in a square array with periodicity $\Lambda_x = \Lambda_y = 1.6\,\mu$m. Coherent bands of strong emissivity ($\varepsilon = 1$) are clearly visible.

In Fig. 4, we show the emissivity (continuous line) for $\vartheta = 0°$ and $d = 4.4\,\mu$m. It is noted a comb of coherent emissivity lines around 10.6 μm. The figure also reports for comparison the normalized absolute value of the polarizability of the single particle (dashed line). We note that the reflectance of the structure is enhanced at the resonance of the single

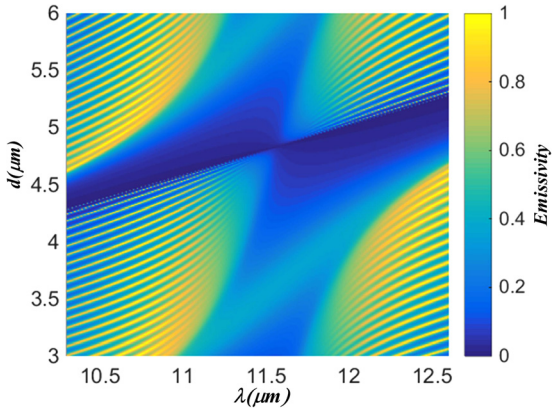

FIG. 3. Emissivity vs. λ and d. Structure parameters are $N = 25$, $\Lambda_x = \Lambda_y = 1.6\,\mu$m, and $r_s = 500$ nm.

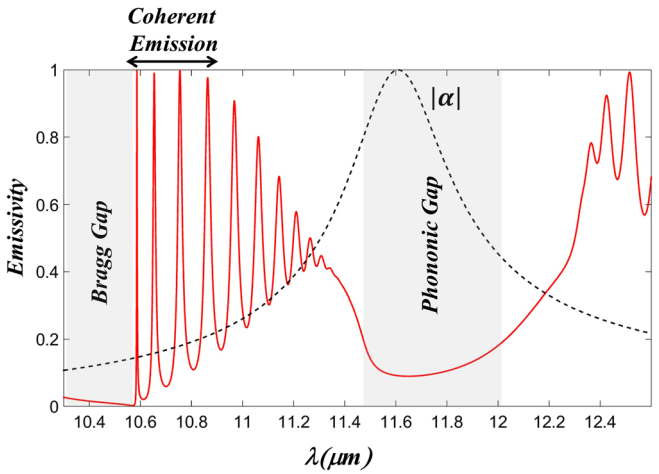

FIG. 4. Emissivity (continuous line) and normalized absolute value of the polarizability of the single particle (dashed line) vs. λ for $d = 4.4\,\mu$m. The other structure parameters are the same as reported in the caption of Fig. 3. The shaded regions indicate, respectively, the conventional Bragg gap of the multilayer and the phononic gap.

particle polarizability ($\lambda_{res} = 11.6\,\mu$m), and therefore the emissivity is quenched. An intrinsic "phononic band gap" is formed due to the excitation of the phonon-polariton on the single particles. This intrinsic phononic band gap is accompanied on the high frequency side by the conventional Bragg gap of the multilayer. The comb of coherent emissivity lines is located in between the phononic band gap and the conventional Bragg gap of the multilayer, the most coherent line being the one located at the band-edge of the Bragg-gap, in close analogy with conventional Bragg gratings[19] where the enhancement of the density of modes at the band edge causes the formation of narrow-band resonances.

For comparison, the emissivity of a uniform *SiC* layer, grown on a metallic mirror and with same thickness as the particle array (1 μm), would be more than one order of magnitude less intense and completely incoherent in the same spectral range, as shown in Fig. 5.

In Fig. 6 it is shown the emissivity as function of the wavelength (λ) and the emission angle (ϑ) for TE and TM polarizations. It is noted that while the Bragg gap undergoes a blue-shift in its spectral position for increasing incident angle, as in conventional multilayer structures, the spectral position of the phononic gap is much less sensitive to the

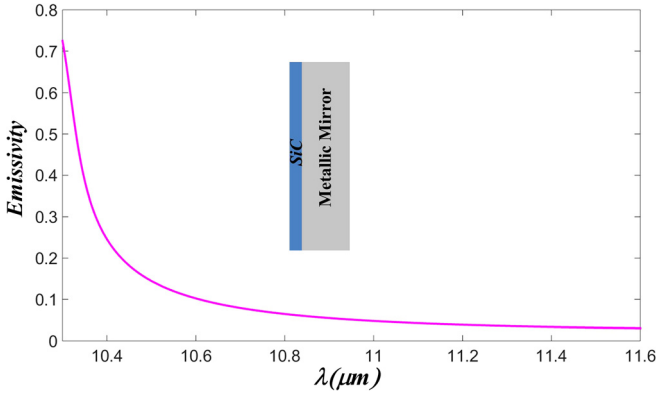

FIG. 5. Emissivity vs. wavelength for a 1 μm thick, uniform *SiC* layer grown on a metallic mirror.

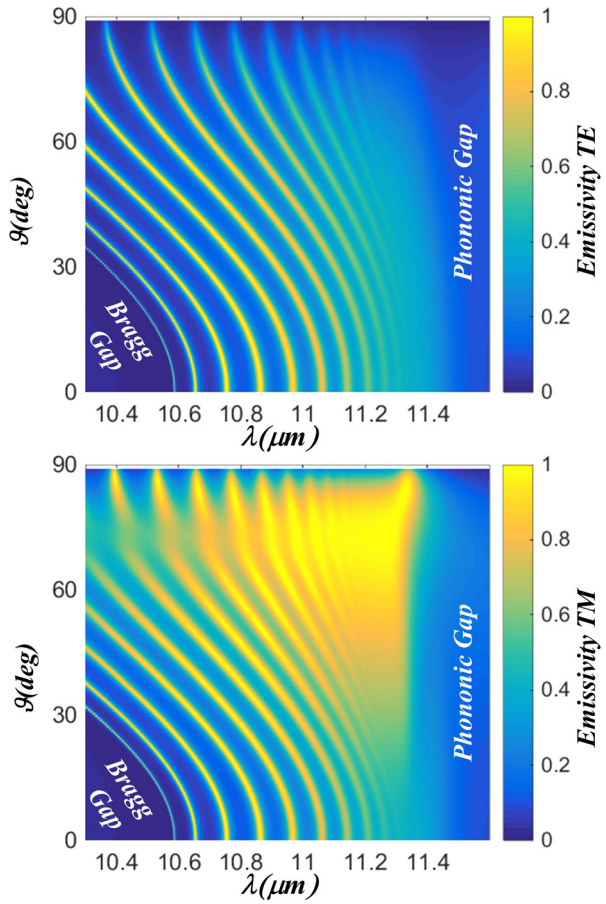

FIG. 6. Emissivity vs. wavelength (λ) and emission angle (ϑ) for TE and TM polarization.

incident angle. This is a typical signature of the phononic nature of the gap and it is ultimately linked to the fact that the resonance of the single particle polarizability α is independent of the incident angle of the forcing field.

In order to draw some quantitative conclusions on the effectiveness of the process, we calculate the Directional Spectral Emissive Power (DSEP) and the Integrated DSEP (IDSEP) defined, respectively, as[2]

$$DSEP\left(\frac{W}{m^2 \times \mu m \times sr}\right) = \varepsilon(\lambda,\vartheta)\cos(\vartheta) I_{\lambda b},$$
$$IDSEP\left(\frac{W}{m^2 \times sr}\right) = \int_{\Delta\lambda} \varepsilon(\lambda,\vartheta)\cos(\vartheta) I_{\lambda b} d\lambda, \qquad (5)$$

where $I_{\lambda b} = (2hc^2/\lambda^5)\left[e^{\frac{hc}{K_B T\lambda}} - 1\right]^{-1}$ is the black-body intensity distribution function, $\varepsilon(\lambda,\vartheta)$ is the total emissivity as defined in Eq. (4), h is Planck's constant, K_B is Boltzmann's constant, and T is the body temperature in Kelvin. The integration is carried over the bandwidth $\Delta\lambda$ of the emissivity line. We also calculate the coherence length of the emission $l_c \sim \lambda^2/\Delta\lambda_{FWHM}$, where $\Delta\lambda_{FWHM}$ is the bandwidth at the full-width half-maximum. The results are shown in Fig. 7 for structures of different periods supposing a temperature of 1000 K. Here, we concentrate only on the band-edge resonance.

The coherence length of the emission scales as N^2 while the Integrated Directional Spectral Emissive Power scales as N^{-2}, this means that there is a trade-off between the available

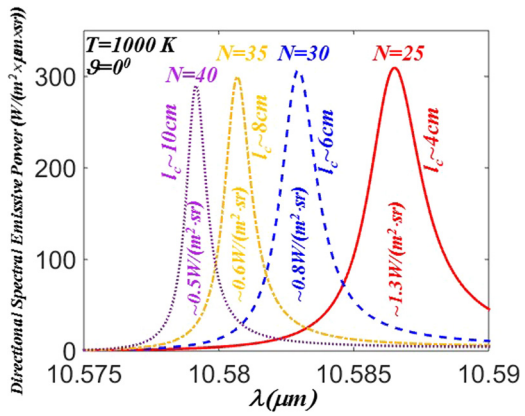

FIG. 7. Band-edge resonance directional spectral emissive power at 0° vs. wavelength for different number of layers. The corresponding approximate values of the integrated directional spectral emissive power are reported under the respective resonances. In the figure are also reported the respective approximate coherence lengths.

power emitted at a certain wavelength and the coherence length of the radiation. The optimal choice will at the end depend on the particular application sought. For example, a radiant surface of 1 m^2 and $N = 120$ layers at $T = 1000$ K can generate an average power of $\sim$50 mW with a coherence length of $\sim$1 m. Such power can be, for example, focused over a $\sim 100\,\mu m^2$ area of a particular material giving rise to an average local intensity of $\sim$0.1 MW/cm^2, which is enough to excite nonlinear effects or to damage the material. Adding more periods will increase the coherence length at the expense of the emitted power.

In conclusion, we have studied the thermal emissive properties of periodic multilayer arrays of subwavelength particles made of *SiC* embedded in a *ZnSe* host medium and shown the concrete possibility to achieve efficient and coherent thermal emission in the long-wave IR around 10.6 μm. The coherent lines of thermal emission are located in between the Bragg gap of the multilayer and the intrinsic phononic gap. We expect that similar results may also be obtained using other polar materials, such as *BeO*, *AlN*, *GaN*, *MgO*, and *ZnO*, in their respective Reststrahlen band, provided that the sample is designed so that the band edge of the Bragg gap is close enough to the phonon-polariton resonance of the single particle.

I thank Nadia Mattiucci for helpful discussions.

[1]*Mid-Infrared Coherent Sources and Applications*, edited by M. Ebrahim-Zadeh and I. T. Sorokina (Springer, Dordrecht, 2008).
[2]J. R. Howell, R. Siegel, and M. P. Mengüç, *Thermal Radiation Heat Transfer*, 5th ed. (CRC Press, 2011).
[3]J.-J. Greffet, R. Carminati, K. Joulain, J.-P. Mulet, S. Mainguy, and Y. Chen, "Coherent emission of light by thermal sources," Nature **416**(6876), 61–64 (2002).
[4]J. Le Gall, M. Olivier, and J.-J. Greffet, "Experimental and theoretical study of reflection and coherent thermal emission by a SiC grating supporting a surface-phonon polariton," Phys. Rev. B **55**(15), 10105–10114 (1997).
[5]C.-M. Wang, Y.-C. Chang, M.-W. Tsai, Y.-H. Ye, C.-Y. Chen, Y.-W. Jiang, Y.-T. Chang, S. C. Lee, and D. P. Tsai, "Reflection and emission properties of an infrared emitter," Opt. Express **15**(22), 14673–14678 (2007).
[6]G. Biener, N. Dahan, A. Niv, V. Kleiner, and E. Hasman, "Highly coherent thermal emission obtained by plasmonic bandgap structures," Appl. Phys. Lett. **92**(8), 081913 (2008).
[7]M. Laroche, R. Carminati, and J.-J. Greffet, "Coherent thermal antenna using a photonic crystal slab," Phys. Rev. Lett. **96**(12), 123903 (2006).
[8]X. Liu, T. Tyler, T. Starr, A. F. Starr, N. M. Jokerst, and W. J. Padilla, "Taming the blackbody with infrared metamaterials as selective thermal emitters," Phys. Rev. Lett. **107**(4), 045901 (2011).
[9]N. Mattiucci, G. D'Aguanno, A. Alu', C. Argyropoulos, J. V. Foreman, and M. J. Bloemer, "Taming the thermal emissivity of metals: A metamaterial approach," Appl. Phys. Lett. **100**, 201109 (2012).
[10]G. D'Aguanno, N. Mattiucci, A. Alù, C. Argyropoulos, J. V. Foreman, and M. J. Bloemer, "Thermal emission from a metamaterial wire medium slab," Opt. Express **20**, 9784–9789 (2012).
[11]M. C. Larciprete, A. Belardini, R. Li Voti, and C. Sibilia, "Pre-fractal multilayer structure for polarization-insensitive temporally and spatially coherent thermal emitter," Opt. Express **21**, A576–A584 (2013).
[12]G. D'Aguanno, N. Mattiucci, M. J. Bloemer, R. Trimm, N. Aközbek, and A. Alù, "Frozen light in a near-zero index metasurface," Phys. Rev. B **90**, 054202 (2014).
[13]G. D'Aguanno and N. Mattiucci, "Dispersive and scattering properties of multilayer arrays made of plasmonic nanoparticles," J. Opt. Soc. Am B **31**, 2524–2530 (2014).
[14]W. G. Spitzer, D. Kleinman, and J. Walsh, "Infrared properties of hexagonal silicon carbide," Phys. Rev. **113**, 127 (1959).
[15]B. Tatian, "Fitting refractive-index data with the Sellmeier dispersion formula," Appl. Opt. **23**, 4477–4485 (1984), see http://refractiveindex.info/.
[16]B. T. Draine, "The discrete-dipole approximation and its application to interstellar graphite grains," Astrophys. J. **333**, 848–872 (1988).
[17]S. A. Maier, *Plasmonics: Fundamentals and Applications* (Springer, New York, 2007).
[18]P. B. Johnson and R. W. Christy, "Optical constants of the noble metals," Phys. Rev. B **6**, 4370–4379 (1972).
[19]G. D'Aguanno, N. Mattiucci, M. Scalora, M. J. Bloemer, and A. M. Zheltikov, "Density of modes and tunneling times in finite one-dimensional photonic crystals: A comprehensive analysis," Phys. Rev. E **70**, 016612 (2004).